Performance Comparison between Coherent and Non-Coherent Approaches for Over-the-Air Computation

Yejin Lee, *Graduate Student Member, IEEE*, Jijun Hwang, *Graduate Student Member, IEEE*, In-Ho Lee, *Senior Member, IEEE*, Haejoon Jung, *Senior Member, IEEE* and Trung Q. Duong, *Fellow, IEEE*

***Abstract*—Over-the-air computation (OAC) can effectively support rapid data aggregation from a plethora of devices, exploiting the inherent superposition property of wireless multiple access channels. The key challenge in OAC is the synchronization of multiple devices, which are handled through either the coherent approach using the beacon transmissions by the fusion center or the non-coherent approach based on random sequences. Motivated by the lack of a fair comparison in prior arts, we derive the closed-form expressions of their mean squared errors (MSEs), which provides an explicit guideline on which approach to use and how we improve one compared to the other by adjusting their key design factors. Thus, this paper provides design insights into the OAC synchronization method depending on the system requirements in terms of MSE.**

***Index Terms*—Over-the-air computation, synchronization, mean squared error, zero-forcing, minimum mean square error.**

I. Introduction

Exploiting the superposition property of wireless multiple access channels, over-the-air computation (OAC) can provide rapid and efficient data aggregation from a large number of devices [1]. In OAC, while multiple devices transmit simultaneously via the same wireless resources, nomographic functions of information at the devices can be computed by appropriate pre- and post-processing with considerably reduced resource usage compared to the conventional schemes [2]. Further, in unmanned aerial vehicle (UAV)-aided OAC, the mobility of UAVs can be exploited to facilitate data aggregation from a myriad of ground-based devices [3].

However, as noted in [4], when it comes to the implementation of OAC, the transmit time synchronization of multiple devices is critical, because the timing error across multiple devices may cause significant distortion of the combined data at the fusion center (FC). In literature, the synchronization methods can be classified into *coherent* and *non-coherent* approaches. In the coherent OAC, as in [3] and [5], each device synchronizes itself based on periodic beacon signals transmitted by the FC. It can ensure constructive signal superposition, but is highly subject to estimation errors of the channel state information (CSI). In particular, phase offsets (POs) pose a significant challenge in practice, due to timing offsets (TOs), phase noise, carrier frequency offsets (CFOs), uplink-downlink channel mismatch, and other impairments [1]. Hence, it is also difficult to analytically characterize the phase error distribution and the corresponding impact on the OAC performance. In contrast, the non-coherent OAC techniques provide robustness against the POs, which include the energy detection [6], frequency shift keying-based majority vote [7], and a continuous-valued OAC over a digital scheme [8].

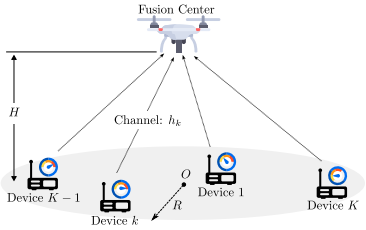

Fig. 1. System model.

Because of their distinct pros and cons, the choice between the two approaches depends on the specific requirements and constraints of a given system or application. However, the existing literature has not explicitly compared the two OAC strategies in terms of mean squared error (MSE) performance, which depends on various system parameters, including phase error and coordination aspects. Motivated by this limitation, in this paper we consider the fair comparison of the two approaches. For the non-coherent approach, we focus on the method in [6], which aims at continuous value aggregation, for a fair comparison with coherent approaches. A comparison with other non-coherent OAC techniques (e.g., [7], [8]) is deferred for a future study. The original contributions can be summarized as follows.

- To the best of our knowledge, this is the first study to fairly compare coherent and non-coherent OAC. Assuming an OAC network with one FC and a large number of devices, we clarify their differences in raw data normalization (or dynamic range of the encoded data), pre-processing at each device (i.e., transmit coefficients), and post-processing at the FC (e.g., denoising factors and offsets).
- We derive the MSEs of both approaches in closed-form expressions, considering both zero-forcing (ZF) and minimum mean square error (MMSE) coordination, using the same theoretical framework. This process provides explicit guidance in each scenario on which to use and

Y. Lee, J. Hwang, and H. Jung are with the Department of Electronics and Information Convergence Engineering, Kyung Hee University, Yongin 17104, Korea (e-mail: {vexia, jijun170, haejoonjung}@khu.ac.kr)

I.-H. Lee is with the School of Electronic and Electrical Engineering, Hankyong National University, Anseong-si, 17579, Korea (e-mail: ihlee@hknu.ac.kr)

T. Q. Duong is with the Faculty of Engineering and Applied Science, Memorial University, St. John's, NL A1C 5S7, Canada, and with the School of Electronics, Electrical Engineering and Computer Science, Queen's University Belfast, BT7 1NN Belfast, U.K., and also with the Department of Electronic Engineering, Kyung Hee University, Yongin-si, Gyeonggi-do 17104, South Korea (e-mail: tduong@mun.ca).

This work was supported by the MSIT, Korea, in part under the NRF grants (RS-2023-00303757) and in part under the IITP grants (IITP-2024-2021-0-02046).

how to improve one over the other for given system parameters. For coherent OAC, we estimate the probability density function (PDF) for the composite POs, taking into account various factors that cause phase errors. On the other hand, the derived MSE for the non-coherent approach shows how it varies with sequence length.
- Lastly, we present simulation results to investigate the effects of various system parameters on the MSE of both methods.

II. System Model

As shown in Fig. 1, we consider an OAC system with K ground devices uniformly distributed over the disk on the ground with radius R and an FC with height H. The distance of the kth device from the origin O is denoted by r_k, and the angle with respect to the x-axis on the ground is φ_k, where $0 < r_k < R$ and $-\pi < \varphi_k < \pi$. Additionally, the position of the FC is given in cylindrical coordinates as (A, ϕ, H). The distance d_k between the FC and the kth device is given by $d_k = \sqrt{A^2 + r_k^2 - 2Ar_k\cos(\phi - \varphi_k) + H^2}$. The FC aggregates the sensor data measured by the K devices. Due to space and power constraints, we assume that the FC and the devices are equipped with a single antenna.

Let $h_k = \alpha_k e^{j\theta_k}$ be the complex baseband-equivalent channel between the kth device for $k \in \{1, ..., K\}$ and the FC, assuming a line-of-sight (LoS) channel between the FC and devices, where $\alpha_k = |h_k| = \frac{1}{d_k}$ and $\theta_k = \angle h_k = -\frac{2\pi d_k}{\lambda}$. Without loss of generality, we assume that $\alpha_1 \leq \alpha_2 \leq ... \leq \alpha_{K-1} \leq \alpha_K$. At the FC, the function of interest (FoI) is the arithmetic mean as $f = \frac{1}{K}\sum_{k=1}^{K} m_k$, where m_k is the original sensing data collected from the kth device. It is assumed that m_k is uniformly distributed from $m_{\min}$ and $m_{\max}$, where $\Delta = m_{\max} - m_{\min}$. As in [5], the sensing data are independently and identically distributed (i.i.d.) for different k. In digital modulation, the transmitted signal can be represented as a complex number, where the sensing data is mapped into both real and imaginary components [9]. However, because we consider analog amplitude or energy modulation OAC schemes; thus, the sensor readings are assumed to be real-valued, as in [3], [5], [6], [10]. In the following sub-sections, we treat coherent and non-coherent OAC strategies.

A. Coherent Approach

In the coherent strategy, as in [3] and [5], each device estimates its channel gain in a distributed manner using the beacon signal transmitted by the FC. In other words, the multiple devices independently synchronize themselves based on the reference signal sent by the FC. Through this synchronization, the FC can receive the coherent superposition of the multiple signals transmitted from the K devices, which is expressed as

$$y = \sum_{k=1}^{K} h_k b_k s_k + w, \tag{1}$$

where $s_k = \Psi(m_k)$ denotes the normalized measurement data to satisfy $|s_k| \leq 1$. Also, w is the additive white Gaussian noise (AWGN) following a complex Gaussian distribution with the zero-mean and variance of σ^2.

Further, as in [3] and [11], the transmit coefficient b_k for the coherent OAC is given by $b_k = \sqrt{p_k}e^{-j\theta_k}$, where p_k represents the transmit power of the kth node. Because the phases of the received signals from K nodes are coherently combined by the phase alignment (i.e., $\angle h_k b_k = 0$), the dynamic range of the normalized data is given by $-1 \leq s_k \leq 1$. Thus, the normalization function is

$$s_k = \Psi(m_k) = \frac{2m_k}{\Delta} - \frac{m_{\max} + m_{\min}}{\Delta}, \tag{2}$$

where both negative and positive values of s_k can be fully utilized. With the channel inversion method, which is widely used in OAC, as in [5] and [11], the kth node's transmit power is given by $p_k = P\alpha_1^2/\alpha_k^2$, where P is a constant that indicates the maximum transmit power. Also, α_1^2/α_k^2 is the normalization factor to compensate for disparate channel gains of different devices. In other words, the transmit power of the node with the smallest channel gain α_1 becomes P, whereas the other nodes have transmit powers less than or equal to P. The devices are constrained to set their average transmission power not to exceed a maximum power limit, denoted as P. This implies that, over a period during which the channel conditions are approximately constant, the transmission signal of each device satisfies the specified power constraint.

From the received signal in (1), the FC performs the post-processing to achieve the estimated FoI $\hat{f}$ as

$$\hat{f} = \zeta\frac{y}{K} + \frac{m_{\max} + m_{\min}}{2}, \tag{3}$$

where the scaling factor ζ is further discussed in Section III-A.

B. Non-Coherent Approach

Now, we consider the non-coherent OAC strategy proposed in [6] and [12]. This non-coherent approach requires only coarse block-level synchronization, where the measurement information is encoded into N symbols with random phase dithering. Thus, as long as the frames transmitted by K devices, each of which consists of N repetitions of the same measured data (i.e., s_k) with the random phase rotations, have sufficiently large overlaps with each other, the measured data can be retrieved at the FC based on the aggregate received power over multiple symbols.

In non-coherent OAC, the channel phase $\theta_k[n]$ is not estimated, and since the average power must be matched, it is assumed that each device knows the magnitude $\alpha_k[n]$ required to compensate for different path losses. The devices create their own sequences with constant envelopes and random phase dithering. For example, the sequence of the kth device is $[e^{jX_k[1]}, e^{jX_k[2]}, ..., e^{jX_k[N]}]^T \in \mathbb{C}^N$, where $n \in \{1, ..., N\}$ is the sequence index. Also, $X_k[n]$ is i.i.d. for different k and n, following the uniform distribution between 0 and 2π in radian. Then, the FoI is obtained by combining the N received sequences at the FC. Therefore, the received signal at time slot (or sequence index) n is

$$y[n] = \sum_{k=1}^{K} h_k b_k[n] s_k + w[n], \tag{4}$$

where the channel h_k is assumed to be quasi-static (i.e., time-invariant for N sequence transmissions)). Also, $b_k[n]$ denotes the transmit coefficient of the kth device at the nth sequence, while s_k is the encoded data of the kth device. In addition, $w[n]$ is the AWGN at the nth time slot with the zero mean and variance of σ^2.

Further, in contrast to the coherent scheme, the encoded data s_k cannot be negative, because positive and negative data cannot be distinguished due to the lack of phase synchronization. As a result, the dynamic range of the normalized data is given by $0 \leq s_k \leq 1$. Thus, the normalization function, which converts the raw measurement data m_k into s_k, is given by

$$s_k = \Psi(m_k) = \sqrt{\frac{m_k}{\Delta} - \frac{m_{\min}}{\Delta}}. \tag{5}$$

The transmit coefficient for OAC is given by $b_k[n] = \sqrt{p_k} e^{jX_k[n]}$, where the transmit power of the kth node is given by $p_k = P'\alpha_1^2/\alpha_k^2$. For fair comparison for the two methods for a given network topology (or channel gains), we set $P' = \frac{3}{2}P$, because $\mathbb{E}[|s_k|^2] = \frac{1}{3}$ for coherent, while $\mathbb{E}[|s_k|^2] = \frac{1}{2}$ for non-coherent. The FC applies the post-processing to recover the FoI as

$$\hat{f} = \zeta \frac{1}{K} \sum_{n=1}^{N} |y[n]|^2 + m_{\min} - \frac{\Delta}{P'K\alpha_1^2}\sigma^2, \tag{6}$$

where ζ for the non-coherent scheme will be presented in Section III-B.

III. MSE Analysis

Now, in the first two sub-sections, we will analyze the MSEs of both coherent and non-coherent OAC with ZF and MMSE schemes, when the FoI is the arithmetic mean. For the coherent OAC, we consider the impact of the imperfect phase estimation. We also derive the MSE of the non-coherent OAC in [6] as a function of various system parameters including the random sequence length N.

A. Coherent Approach

While the channel magnitude can be estimated using various methods including location information for the ground-to-air channel, the phase estimation is challenging. Thus, with POs caused by TOs, phase noise, CFOs, in-phase and quadrature-phase imbalance (IQI), the UAV (i.e., FC) jittering effects, and other impairments, the transmit coefficient b_k for the k device becomes $b_k = \sqrt{p_k} e^{-j(\theta_k + e_k)}$, where e_k is the PO of the kth node. It is assumed that the errors for different devices (i.e., e_k with $k \in \{1, ..., K\}$) are i.i.d. Because there are various factors causing phase offset in practical communication systems [13]–[16], it is advantageous to confirm it clearly through hardware implementation such as software-defined radio (SDR) platforms [1]. However, in practice, SDR platform hardware exists with different architectures, performances, costs, and sizes, by which the POs may be characterized differently depending on specific hardware (or testbed) configurations. As a result, it is challenging to integrate all of the system-level impairments into a single random variable with a closed-form PDF for theoretical analysis. Therefore, in this paper, we model POs using the non-parametric kernel estimation method and analyze the MSE. This method calculates the PDF through sampling and is widely used in the field of communications [17]–[21]. For example, in [19], when characterizing the objective function in blind signal separation, the PDF for blind signals is obtained using Gaussian kernel-based non-parametric estimation. Also, in [17], for regularized particle filtering, the kernel density method is used to solve the particle impoverishment problem. Moreover, since the PDF is estimated through sampling, the proposed closed-form equations can be directly applied even for other factors in the future. Especially, because the Gaussian kernel is distributed over the entire range of the axis and has the smoothest form, it is the most commonly used kernel. Therefore, in this paper, we also model the PDF of the POs using a Gaussian kernel.

In addition, to model composite POs, the random variables for the individual impairments are assumed to be independent of each other. Therefore, the mixture of these random variables is represented by the sum of the random variables, and the estimator can only sample the composite POs as a whole, not each random variable (or PO) caused by an individual impairment. With available sample observations $\{\bar{e}_1, \bar{e}_2, ..., \bar{e}_L\}$, the estimated PDF with the Gaussian kernel is

$$\hat{z}_{e_k}(e) = \frac{1}{\sqrt{2\pi}hL} \sum_{l=1}^{L} \exp\left[-\frac{(e - \bar{e}_l)}{2h^2}\right], \tag{7}$$

where L is the size of the set and $-\infty < e < \infty$. Furthermore, the constant for smoothing is given by $h = L^{\delta}(L-1)\sigma_e$, where σ_e is the standard deviation from the survey set and δ is an empirical constant.

1) ZF Coordination: As in [3], [5], [22], for the ZF coordination that ignores the additive noise, the coherent denoising factor is designed as $\zeta = \frac{\Delta}{2\sqrt{P}\alpha_1}$. The following proposition provides the corresponding MSE.

Proposition 1: The MSE of the coherent OAC with the ZF coordination is given by

$$\texttt{MSE} = \frac{\Delta^2}{6K}\left(1 - \mathbb{E}[\cos(e_k)]\right) + \frac{\Delta^2\sigma^2}{4P\alpha_1^2K^2}. \tag{8}$$

Proof: From the estimated FoI $\hat{f}$, the MSE is computed as

$$\begin{aligned}\texttt{MSE} = \mathbb{E}\left[\left|\hat{f} - f\right|^2\right] &= \frac{\mathbb{V}\mathrm{ar}[m_k](2 - 2\,\mathbb{E}[\cos(e_k)]) + \frac{\Delta^2\sigma^2}{4P\alpha_1^2K}}{K} \\ &= \frac{\Delta^2}{6K}\left(1 - \mathbb{E}[\cos(e_k)]\right) + \frac{\Delta^2\sigma^2}{4P\alpha_1^2K^2}. \end{aligned} \tag{9}$$

■

It is noted that, we can simplify (8) with $\mathbb{E}[\cos(e_k)] = \exp\left[-\frac{1}{2}h^2\right]\frac{1}{L}\sum_{l=1}^{L}\cos(\bar{e}_l)$ with Gaussian kernel. If a different kernel is employed, the corresponding $\mathbb{E}[\cos(e_k)]$ can be readily computed [23]. Based on Proposition 1, we can identify the following key properties of the MSE, which show the impacts of important system parameters. First, as the transmit power of the devices, P, increases, the MSE decreases, because of the reduced noise-related term $\frac{\Delta^2\sigma^2}{4P\alpha_1^2K^2}$ in (8). Also, even with infinite power, the MSE has a non-zero limiting value as $\lim_{P\to\infty}\texttt{MSE} = \frac{\Delta^2}{6K}\left(1 - \mathbb{E}[\cos(e_k)]\right)$, which

is the PO terms. In other words, even with infinite P, the distortion by the phase estimation error cannot be overcome. Moreover, as K increases, the MSE decreases. Moreover, when $K \to \infty$, $\texttt{MSE} \to 0$.

2) MMSE Coordination: In this part, we derive the post-processing factor ζ for the MMSE coordination that minimizes the MSE. First, to obtain the MSE, we compute

$$\hat{f} - f = \frac{1}{K}\left[\zeta \sum_{k=1}^{K} h_k b_k s_k + \zeta w - \sum_{k=1}^{K} m_k\right] + \frac{m_{\max} + m_{\min}}{2} = \frac{1}{K}\left[\sum_{k=1}^{K} (\zeta h_k b_k - \frac{\Delta}{2}) s_k + \zeta w\right]. \quad (10)$$

Since $\mathbb{E}[s_k] = 0$ and $E[|s_k|^2] = 1/3$, the MSE is given by

$$\texttt{MSE} = \mathbb{E}[|\hat{f} - f|^2] = \frac{1}{K^2}\mathbb{E}\left[\left(\sum_{k=1}^{K} |(\zeta h_k b_k - \frac{\Delta}{2}) s_k|^2\right) + \zeta^2 w^2\right]. \quad (11)$$

Thus, we can formulate an optimization problem to minimize the MSE as

$$\min_{\zeta, b_k} \frac{1}{K^2}\mathbb{E}\left[\left(\sum_{k=1}^{K} |(\zeta h_k b_k - \frac{\Delta}{2}) s_k|^2\right) + \zeta^2 w^2\right]. \quad (12)$$

In general, this optimization problem is non-convex and difficult to solve; thus, it is typically tackled by an iterative algorithm to optimize ζ and b_k [24], [25]. The optimal b_k typically follows a threshold-based regularized channel inversion structure [24], [25]. Moreover, because the closed-form analytical solution is not available through the joint optimization of ζ and b_k in an iterative manner, we find the optimal solution for ζ by fixing b_k as the channel inversion policy to derive the closed-form expression of MSE, as in [24]. Consequently, the optimal ζ, which corresponds to $\frac{\partial \texttt{MSE}}{\partial \zeta} = 0$ and $\frac{\partial^2 \texttt{MSE}}{\partial \zeta^2} > 0$, can be obtained as

$$\zeta = \frac{\Delta\sqrt{P}\alpha_1 \mathbb{E}[\cos(e_k)]}{2P\alpha_1^2 + \frac{6\sigma^2}{K}} = \frac{\Delta \mathbb{E}[\cos(e_k)]}{2\sqrt{P}\alpha_1 + \frac{6\sigma^2}{\sqrt{P}\alpha_1 K}}. \quad (13)$$

The corresponding MSE can be readily obtained in the following proposition.

Proposition 2: The MSE of the coherent OAC with the MMSE coordination can be expressed as

$$\texttt{MSE} = \frac{\Delta^2}{12K} - \left(\frac{\Delta^2 \mathbb{E}[\cos(e_k)]^2}{12K + 36\frac{\sigma^2}{P\alpha_1}}\right). \quad (14)$$

Accordingly, we can observe the following properties for the MSE with the MMSE coordination. As the maximum power for the coherent OAC P increases, the MSE in (14) decreases. Moreover, even when $P \to \infty$, the MSE does not converge to zero as $\lim_{P\to\infty} \texttt{MSE} = \frac{\Delta^2}{12K}\left(1 - \mathbb{E}[\cos(e_k)]^2\right)$. Only in the absence of the POs (i.e., $e_k = 0$ for any k), which corresponds to $\mathbb{E}[\cos(e_k)] = 1$, the limiting MSE for infinite P becomes zero.

B. Non-Coherent Approach

In this subsection, we analyze the MSE of the non-coherent OAC for both ZF and MMSE schemes.

1) ZF Coordination: First, we consider the original non-coherent approach in [6] with N repetitions of a random phase sequence, where $\zeta = \frac{\Delta}{P' N \alpha_1^2}$ in (6).

Proposition 3: The MSE of the non-coherent OAC with $\zeta = \frac{\Delta}{P' N \alpha_1^2}$ is expressed as

$$\texttt{MSE} = \frac{\Delta^2}{NK}\Big(\frac{K-1}{4} + \frac{\sigma^2}{2P'\alpha_1^2} + \frac{\sigma^4}{P'^2 K \alpha_1^4}\Big). \quad (15)$$

Proof: Suppose $\mathcal{S} = \sum_{n=1}^{N} |y[n]|^2$ in (6). Then, we have

$$\mathcal{S} = \sum_{n=1}^{N} |\sum_{k\in\mathcal{K}} h_k b_k[n] s_k + w[n]|^2 = \underbrace{\sum_{n=1}^{N}\sum_{k=1}^{K}\sum_{\substack{i=1\\ j\neq k}}^{K} P'\alpha_1^2 \sqrt{\frac{m_k - m_{\min}}{\Delta}\frac{m_i - m_{\min}}{\Delta}} e^{j(\tilde{X}_i[n] - \tilde{X}_k[n])}}_{=:\mathcal{A}} + \underbrace{2\sum_{n=1}^{N}\sum_{k=1}^{K}\sqrt{P'}\alpha_1\sqrt{\frac{m_k}{\Delta} - \frac{m_{\min}}{\Delta}}\Re\Big\{e^{j\tilde{X}_k[n]} w^*[n]\Big\}}_{=:\mathcal{B}} + \underbrace{\sum_{n=1}^{N}|w[n]|^2}_{=:\mathcal{C}} + N\sum_{k=1}^{K} P'\alpha_1^2(\frac{m_k}{\Delta} - \frac{m_{\min}}{\Delta}). \quad (16)$$

Because $\tilde{X}_i[n] - \tilde{X}_k[n]$ follows the uniform distribution in $[0, 2\pi]$ for $i \neq k$, we have $\mathbb{E}[\mathcal{A}] = 0$ and the variance as

$$\mathbb{V}\text{ar}[\mathcal{A}] = \frac{1}{4} P'^2 \alpha_1^4 NK(K-1). \quad (17)$$

Moreover, because $w[n]$ follows the complex Gaussian distribution with zero mean and variance of σ^2, we obtain $\mathbb{E}[\mathcal{B}] = 0$ while its variance is given by

$$\mathbb{V}\text{ar}[\mathcal{B}] = P' N \alpha_1^2 \sigma^2 \sum_{k=1}^{K} \mathbb{E}\left[\frac{m_k}{\Delta} - \frac{m_{\min}}{\Delta}\right] = \frac{1}{2} P' N K \alpha_1^2 \sigma^2.$$

Lastly, we can readily obtain $\mathbb{E}[\mathcal{C}] = N\sigma^2$ and $\mathbb{V}\text{ar}[\mathcal{C}] = N\sigma^4$. Therefore, the MSE of the non-coherent OAC is simplified as

$$\texttt{MSE} = \mathbb{E}\left[\left|\hat{f} - f\right|^2\right] = \mathbb{E}\left[\left|\zeta\frac{1}{K}\mathcal{S} + m_{\min} - \frac{\Delta}{P' K \alpha_1^2}\sigma^2 - f\right|^2\right] = \frac{\Delta^2}{P'^2 K^2 N^2 \alpha_1^4}\mathbb{E}\left[\left|\mathcal{A} + \mathcal{B} + \mathcal{C} - N\sigma^2\right|^2\right] = \frac{\Delta^2 \mathbb{V}\text{ar}[\mathcal{A} + \mathcal{B} + \mathcal{C}]}{P'^2 K^2 N^2 \alpha_1^4} = \frac{\Delta^2}{NK}\Big[\frac{K-1}{4} + \frac{\sigma^2}{2P'\alpha_1^2} + \frac{\sigma^4}{P'^2 K \alpha_1^4}\Big].$$

■

The MSE in Proposition 3 decreases, as the transmit power P', increases. However, even with infinite P', the MSE has the non-zero limiting value as $\lim_{P'\to\infty} \texttt{MSE} = \frac{\Delta^2(K-1)}{4NK}$. In addition, as the number of devices K increases, $\frac{\Delta^2}{NK}\left(\frac{\sigma^2}{2P'\alpha_1^2} + \frac{\sigma^4}{P'^2 K \alpha_1^4}\right)$ in (15), which is subject to AWGN, decreases. However, the other term $\frac{\Delta^2(K-1)}{4NK}$ is an increasing

function of K. Also, with infinite K, the MSE has the following limiting value $\lim_{K\to\infty} \texttt{MSE} = \frac{\Delta^2}{4N}$.

2) MMSE Coordination: We adopt the MMSE coordination approach to minimize the MSE, enabling the derivation of a closed-form expression in the non-coherent OAC, similarly to the MMSE coordination for the coherent OAC in Section III-A2. First, we obtain the MSE expression as

$$\begin{aligned}\texttt{MSE} &= \mathbb{E}[|\hat{f}-f|^2] \\ &= \mathbb{E}[|\frac{\zeta}{K}(\mathcal{A}+\mathcal{B}+\mathcal{C})+\frac{\zeta N P'\alpha_1^2-\Delta}{K}\sum_{k=1}^{K} s_k^2-\frac{\Delta}{P'K\alpha_1^2}\sigma^2|^2].\end{aligned}$$

where $\mathcal{S}$ is the same as the ZF case in (16) with the identical $\mathcal{A}$, $\mathcal{B}$ and $\mathcal{C}$. Because $\mathbb{E}[|s_k|^2]=\frac{1}{2}$ and $\mathbb{E}[|s_k^2|^2]=\frac{1}{3}$ for the non-coherent OAC, the MMSE minimization problem becomes

$$\begin{aligned}\min_{\zeta, b_k[n]} \frac{\zeta^2}{K^2}\left(\mathbb{V}\mathrm{ar}[\mathcal{A}+\mathcal{B}+\mathcal{C}]+E[C^2]\right) \\ +\frac{\zeta}{K}(\Delta_1-2\Delta_2)\,\mathbb{E}[\mathcal{C}]+\frac{\Delta_1^2}{3K^2}-\Delta_1\Delta_2+\Delta_2^2, \quad (18)\end{aligned}$$

where $\Delta_1 = \zeta N P'\alpha_1^2 - \Delta$ and $\Delta_2 = \frac{\Delta}{P'K\alpha_1^2}\sigma^2$. Fixing $b_k[n]=\sqrt{p_k}e^{jX_k[n]}$ as defined in Section II-B, we can obtain the optimal ζ, which corresponds to $\frac{\partial\,\texttt{MSE}}{\partial\zeta}=0$ and $\frac{\partial^2\,\texttt{MSE}}{\partial\zeta^2}>0$, in a closed form as

$$\zeta = \frac{4\Delta K(\mathcal{D}^2+3\mathcal{D}\sigma^2+3\sigma^4)}{3\mathcal{D}^3(1-\frac{1}{K}+\frac{4N}{3})+12\mathcal{D}\sigma^2\left((1+2N)(\frac{\mathcal{D}}{2}+\sigma^2)-N\sigma^2\right)}, \quad (19)$$

where $\mathcal{D}=\alpha_1^2KP'$. As a result, the MSE is presented in the following proposition.

Proposition 4: The MSE for the non-coherent OAC with the MMSE coordination is expressed as

$$\texttt{MSE} = \frac{\Delta^2(\mathcal{D}^2+3\mathcal{D}\sigma^2+3\sigma^4)(\mathcal{D}^2(K-1)+2\mathcal{D}K\sigma^2+4K\sigma^4)}{3K\,\mathcal{D}^2(\mathcal{D}^2(1-\frac{1}{K}+\frac{4N}{3})+2\sigma^2((1+2N)(\mathcal{D}+\sigma^2)+\sigma^2))}. \quad (20)$$

Based on Proposition 4, we can identify the following properties of the MSE. First, with higher P', the MSE decreases, ultimately converging to $\lim_{P'\to\infty}\texttt{MSE} = \frac{\Delta^2(K-1)}{-3+K(3+4N)}$ as $P'\to\infty$. Also, as K increases, the MSE approaches the limiting value of $\lim_{K\to\infty}\texttt{MSE}=\frac{\Delta^2}{3+4N}$.

IV. Simulation Results

In this section, we will present simulation results to observe the impacts of various system parameters and validate our analysis. For simulation, we use $m_{\min}=-1$, $m_{\max}=1$, and the carrier frequency is 1GHz. The devices are assumed to be uniformly distributed over the disk with $R=100$m and the height of the FC from the ground H is 200m for the system model in Fig. 1. In addition, for the coherent approach, we consider the composite POs are subject to quantization noise [13], phase estimation error in phase-locked loop (PLL) circuit [14], UAV jittering effect [15], and IQI [16]. Following the corresponding models in [13]–[16], we employ a uniform distribution for quantization noise [13], a

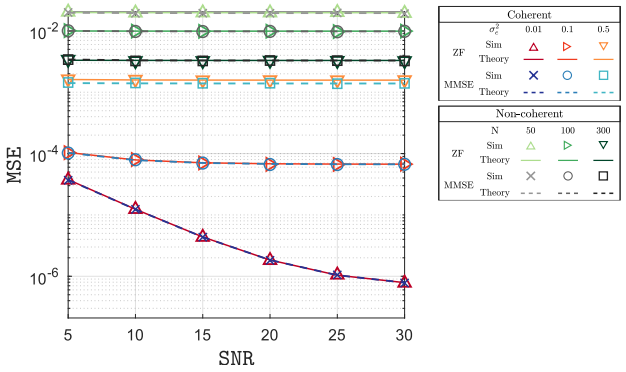

Fig. 2. The MSE performances of coherent and non-coherent OAC, when $B_q=3$, $g_{\min}=1$, $g_{\max}=2$, $K=100$, $\sigma_e^2\in\{0.01,0.1,0.5\}$, and $N\in\{50,100,300\}$.

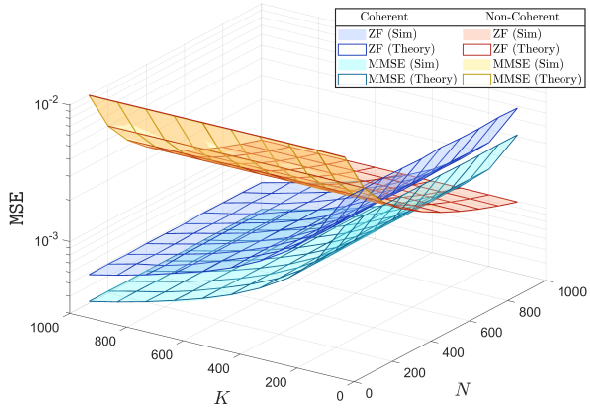

Fig. 3. The MSEs with different K and N, when $\texttt{SNR}=20$dB, $B_q=4$ and $\sigma_e^2=2$.

Tikhonov distribution for PLL [14], and Gaussian distributions for IQI and jittering effect. These factors are assumed to be independent of each other, by which the composite POs are expressed as the sum of these phase errors. Other factors except for the quantization noise are assumed to have the same variance, and the quantization level is defined as B_q. It is noted that the non-parametric estimation method proposed in this paper can be applied to an arbitrary combination of various impairments that affect the POs. To quantify the degree of the composite effects, we define the variance of the composite POs as σ_e^2. Moreover, the estimator randomly samples among the composite POs measured in the entire iteration and computes the PDF from the sample observations. The reliability of the proposed closed-form equation is verified by comparing the simulation and theoretical results.

Fig. 2 shows how the MSEs vary with different average signal-to-noise ratios (SNRs) of the received signal at the FC. In the coherent scenario, the MSE significantly deteriorates, as the variance of the PO σ_e^2 increases. On the other hand, for the non-coherent systems, the MSE decreases, as the sequence length N increases, which is in line with the properties derived from Propositions 3 and 4. Further, the simulation results are consistent with the analytical results for the arithmetic mean, which validate our analysis in the previous section. Also, comparing the ZF and MMSE schemes, MMSE consistently yields equal or lower MSEs compared to ZF for both coherent and non-coherent cases.

In Fig. 3, we investigate the impacts of the number of

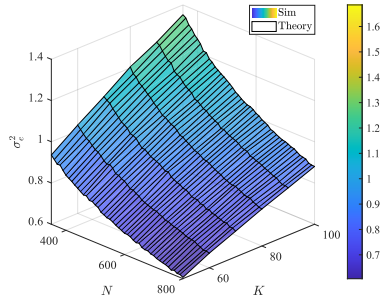

Fig. 4. The variances of the POs σ_e^2 to achieve the same MSEs with ZF, when $\texttt{SNR} = 15$dB and $B_q = 1$.

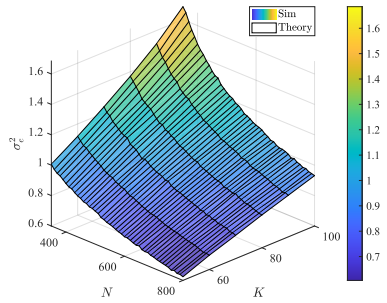

Fig. 5. The variances of the POs σ_e^2 for the same MSEs with MMSE, when $\texttt{SNR} = 15$dB and $B_q = 1$.

devices K and sequence length N on the MSE performance. The MSE of the coherent OAC decreases, as K increases, which shows its effectiveness with massive K. On the other hand, the MSE of the non-coherent OAC decreases, as the random sequence length N increases. We observe that with large enough N, the MSE for the non-coherent OAC can become lower than that for the coherent OAC, which indicates performance improvement by the pertinent choice of the two approaches with parameter adjustments. In addition, for both approaches, MMSE outperforms ZF.

Lastly, Figs. 4 and 5 show the variance of PO σ_e^2 for the coherent OAC to achieve the same MSE as that of the non-coherent OAC for different K and N. It is observed that the required σ_e^2 values of the simulation and analysis are almost the same, meaning that we can determine which approach to use based on the derived MSEs for the given system parameters. In addition, σ_e^2, which gives the same MSEs, decreases, as K decreases. Also, it increases with higher N, because the MSE of the non-coherent OAC improves.

V. Conclusion

In this paper, we have made a fair comparison between the coherent and non-coherent OAC approaches following the same theoretical framework and clarified the differences including the data encoding, pre-processing, and post-processing. Further, the MSEs of both approaches with the ZF and MMSE schemes have been derived in closed-form expressions, which capture how the two MSEs change depending on the key system parameters such as transmit power, channel gain, and the number of devices. In particular, the MSE of the coherent OAC is highly susceptible to the POs, whilst the sequence length is the key factor in that of the non-coherent OAC. In addition, we have presented simulation results to validate our analysis and investigated the impacts of various system parameters.

References

[1] A. Şahin and R. Yang, "A survey on over-the-air computation," *IEEE Commun. Surveys & Tutorials*, vol. 25, no. 3, pp. 1877–1908, Apr. 2023.

[2] G. Shi *et al.*, "Multiple parallel federated learning via over-the-air computation," *IEEE Open J. Commun. Society*, vol. 3, pp. 1252–1264, Jul. 2022.

[3] H. Jung and S.-W. Ko, "Performance analysis of UAV-enabled over-the-air computation under imperfect channel estimation," *IEEE Wireless Commun. Lett.*, vol. 11, no. 3, pp. 438–442, Mar. 2022.

[4] G. Zhu *et al.* "Over-the-air computing for wireless data aggregation in massive IoT," *IEEE Wireless Commun.*, vol. 28, no. 4, pp. 57–65, Apr. 2021.

[5] W. Liu *et al.*, "Over-the-air computation systems: Optimization, analysis and scaling laws," *IEEE Trans. Wireless Commun.*, vol. 19, no. 8, pp. 5488–5502, Aug. 2020.

[6] M. Goldenbaum and S. Stanczak, "Robust analog function computation via wireless multiple-access channels," *IEEE Trans. Commun.*, vol. 61, no. 9, pp. 3863–3877, Sep. 2013.

[7] A. Şahin, "Distributed learning over a wireless network with non-coherent majority vote computation," *IEEE Trans. Wireless Commun.*, vol. 22, no. 11, pp. 8020–8034, Nov. 2023.

[8] ——, "Over-the-air computation based on balanced number systems for federated edge learning," *IEEE Trans. Wireless Commun.*, vol. 23, no. 5, pp. 4564–4579, 2024.

[9] S. Razavikia *et al.*, "ChannelComp: A general method for computation by communications," *IEEE Trans. Commun.*, vol. 72, no. 2, pp. 692–706, Feb. 2024.

[10] S. K. Jha *et al.*, "Fundamental limits of over-the-air optimization: Are analog schemes optimal?" *IEEE J. on Sel. Areas Info. Theory*, vol. 3, no. 2, pp. 217–228, Jun. 2022.

[11] X. Cao *et al.*, "Optimized power control for over-the-air computation in fading channels," *IEEE Trans. Wireless Commun.*, vol. 19, no. 11, pp. 7498–7513, Nov. 2020.

[12] M. Goldenbaum and S. Stanczak, "On the channel estimation effort for analog computation over wireless multiple-access channels," *IEEE Wireless Commun. Lett.*, vol. 3, no. 3, pp. 261–264, Jun. 2014.

[13] A. D. Dabbagh and D. J. Love, "Multiple antenna MMSE based downlink precoding with quantized feedback or channel mismatch," *IEEE Trans. Commun.*, vol. 56, no. 11, pp. 1859–1868, Nov. 2008.

[14] N. C. Beaulieu *et al.*, "Novel theoretical performance comparisons of open-loop and closed-loop timing recovery in Rayleigh fading channels with and without a receiver outage condition," *IEEE Wireless Commun. Lett.*, vol. 8, no. 5, pp. 1448–1451, Oct. 2019.

[15] W. Wang and W. Zhang, "Jittering effects analysis and beam training design for UAV millimeter wave communications," *IEEE Trans. Wireless Commun.*, vol. 21, no. 5, pp. 3131–3146, May. 2021.

[16] Y. Xiong *et al.*, "Channel estimation and IQ imbalance compensation for uplink massive MIMO systems with low-resolution ADCs," *IEEE Access*, vol. 5, pp. 6372–6388, Apr. 2017.

[17] J. Lim and D. Hong, "Gaussian particle filtering approach for carrier frequency offset estimation in OFDM systems," *IEEE Signal Proc. Lett.*, vol. 20, no. 4, pp. 367–370, Apr. 2013.

[18] Q. Yan *et al.*, "Specmonitor: Toward efficient passive traffic monitoring for cognitive radio networks," *IEEE Trans. Wireless Commun.*, vol. 13, no. 10, pp. 5893–5905, Oct. 2014.

[19] H. Yang *et al.*, "Baseband communication signal blind separation algorithm based on complex nonparametric probability density estimation," *IEEE Access*, vol. 6, pp. 22 434–22 440, Apr. 2018.

[20] Q. Z. Ahmed *et al.*, "Bit error-rate minimizing detector for amplify-and-forward relaying systems using generalized gaussian kernel," *IEEE Signal Proc. Lett.*, vol. 20, no. 1, pp. 55–58, Jan. 2012.

[21] T. Kadir and M. Brady, "Non-parametric estimation of probability distributions from sampled signals," Technical report, OUEL, Tech. Rep., Jul. 2005.

[22] H. Hellström *et al.*, "Over-the-air federated learning with retransmissions," *in Proc. IEEE SPAWC*, pp. 291–295, Sep. 2021.

[23] K. N. Plataniotis *et al.*, "Color image processing using adaptive multichannel filters," *IEEE Trans. Image Proc.*, vol. 6, no. 7, pp. 933–949, Jul. 1997.

[24] Y. Chen *et al.*, "Over-the-air computation with imperfect channel state information," *in Proc. IEEE SPAWC*, pp. 1–5, Jul. 2022.

[25] Y.-W. P. Hong and C.-C. Wang, "In-network learning via over-the-air computation in Internet-of-things," *in Proc. IEEE SPAWC*, pp. 141–145, Jul. 2021.